Double photoionization of methane

Gérald Dujardin, Dominique Winkoun, and Sydney Leach
Laboratoire de Photophysique Moléculaire, Université de Paris—Sud, Bâtiment 213, F-91405 Orsay Cédex, France*
and Laboratoire pour l'Utilisation du Rayonnement Electromagnétique, Université de Paris—Sud,*
Bâtiment 209c, F-91405 Orsay Cédex, France
(Received 19 October 1984)

Double photoionization (DPI) of CH_4 has been studied in the photon-energy range 35—52 eV by the photoion-photoion coincidence (PIPICO) method. Throughout this energy range the measured DPI cross section is found to be much smaller than that of the corresponding process in the isoelectronic neon atom. Unlike the case of rare-gas atoms, where the ratio of the double- to single-photoionization cross section attains a constant value at higher energies, this ratio for methane passes through a maximum at about 47 eV. Comparison of experimental with calculated energies of CH_4^{2+} electronic states gives evidence that both triplet ($^3T_1$) and singlet (^1E) states are populated by ejection of two electrons from the $1t_2$ orbital of CH_4. In agreement with the calculations of Siegbahn, our results show that the Franck-Condon factors for excitation of the $^3T_1$ state are spread over a wide energy range ($\cong$2 eV). CH_4^{2+} in its $^3T_1$ state rapidly dissociates (via an indirect process) into $CH_3^+(\tilde{X}^1A_1')+H^+(^1S)$, which is the most favorable dissociation pathway, both energetically and dynamically. At higher excitation energies, CH_4^{2+} in its ^1E state dissociates into the three products $CH_2^+(\tilde{X}^2A_1)+H^+(^1S)+H(^2S)$ with a 5-eV kinetic-energy release. Comparison of experimental PIPICO curves with simulated curves derived on the basis of various fragmentation models leads us to conclude that the ionic fragments CH_2^+ and H^+ are ejected at 180° from each other and that they take almost all the available kinetic energy. This would indicate that the Coulomb repulsion between positive charges plays a dominant role in the process of dissociation into these three fragments.

I. INTRODUCTION

Single photon absorption by an atom or a molecule can lead to the ejection of two valence electrons. As noted elsewhere,[1] this is a major result of electron correlations. Due to their lower symmetry, doubly charged molecular cations have more electronic excited states than the isoelectronic atomic doubly charged cations. There exist, however, specific advantages for studying the double photoionization (DPI) of molecular species, as compared with atoms. In particular, the use of the photoion-photoion coincidence (PIPICO) method[1] makes it possible to identify the excited electronic states of the doubly charged molecular ions produced and to determine the corresponding partial double-photoionization cross sections.

In addition to its interest for electron correlation studies, molecular double photoionization has the peculiarity that the Franck-Condon transition from the neutral produces doubly charged species whose nuclear configurations are often very far from nuclear equilibrium.[1] Thus, doubly charged polyatomic cations produced by DPI are generally unstable species which dissociate into fragments with high kinetic energies. We remark that these dissociative processes play an important role in the selective photochemistry obtained by core ionization of molecules.[2] It is known, indeed, that following core ionization, Auger processes are very efficient processes producing doubly charged cations.

The PIPICO method was first used to study the double photoionization of SO_2.[1] We report in the following, PIPICO studies of formation and dissociation of doubly charged CH_4^{2+} cations.

Both valence-electron[3–5] and core-electron[6–10] ionization of methane have been extensively studied in the past few years. These processes are not only of theoretical interest, but are also important in chemistry and as sources of protons.[11] The CH_4 molecule has tetrahedral geometry in its ground state and its electronic configuration (T_d point-group symmetry) is considered to be as follows, on a single-configuration basis:[3]

$$(1a_1)^2(2a_1)^2(1t_2)^6\ \tilde{X}\,^1A_1\ .$$

Extending the Walsh rules to AH_4 systems, Saturno[12] concluded that whereas CH_4 is tetrahedral, CH_4^{2+} with six valence electrons should be planar in its ground state. This implies a D_{4h} point-group symmetry. Because we are concerned here with vertical ionization processes, the electronic orbital and state symmetries will be given as representations in the T_d point group. Though the object of many searches, stable or metastable CH_4^{2+} cations have never been observed by single-electron-impact mass-spectrometry studies. However, dissociative CH_4^{2+} cations have been observed by several authors. The first observation of the decomposition of CH_4^{2+} into singly charged fragments was done by McCulloh, Sharp, and Rosenstock.[13] They used an electron-ion-ion coincidence method to measure the relative abundances of positive ion pairs ($C^+ + H^+$; $H^+ + CH^+$; $H^+ + CH_2^+$; $H^+ + CH_3^+$; $H_2^{2+} + CH_2^+$) produced by bombardment of CH_4 with

1-keV electrons. Backx and Van der Wiel[14] repeated these measurements, using a different ion-ion coincidence technique, at 10-keV electron impact.

Vertical energies of electronic CH_4^{2+} states produced by double ionization of CH_4 were measured by Auger electron spectroscopy[6] and by double-charge-transfer (DCT) spectroscopy.[15] From a comparison of these energies with those from Hartree-Fock calculations[16,17] it was concluded that the broad, lowest CH_4^{2+} band, observed at 40.7 ± 0.8 eV vertical energy in the Auger experiment and at 38.9 ± 0.7 eV in the DCT experiment, probably corresponds to some of the overlapping multiple states ($^3T_1$, ^1E, $^1T_2$, $^1A_1$) of CH_4^{2+} originating from the ejection of two $1t_2$ electrons. As noted by Clementi and Popkie[16] it is remarkable that there seems to be no need, for the determination of the single and double vertical ionization potentials in CH_4, to perform calculations including electron correlation corrections. This is due to the fact that electron correlation corrections decrease the total energies of CH_4, CH_4^+, and CH_4^{2+} in uniform fashion. This case clearly shows that in order to get evidence for correlation effects in DPI, one needs to consider the DPI cross sections rather than the vertical energies of the doubly charged electronic states.

Interest in the double ionization of methane was recently reinforced by the results of the charge stripping experiment of Ast *et al.*[18] and Rabrenovic *et al.*[19] who found that metastable CH_4^{2+} cations could be formed at a double-ionization energy of 30.6 eV. This result, in apparent contradiction with previous results obtained by Auger and DCT spectroscopy, was explained by several authors[20–22] by considering that double ionization by charge stripping is a two-step process. In the first step, CH_4^+ ions are produced by electron impact on CH_4. Subsequently, in the second step ($CH_4^+ + N_2 \rightarrow CH_4^{2+} + N_2 + e^-$), CH_4^{2+} ions are considered to be produced with a geometry (square planar) very different from that of the CH_4^{2+} ions formed by the vertical transition from the tetrahedral neutral CH_4 which occurs in Auger and DCT experiments. One can thus expect that, by charge stripping, one reaches a part of the CH_4^{2+} $^1A_1$ potential surface which is near the local minimum of this surface, whereas by vertical transition from CH_4 one reaches the dissociative part of the $^3T_1$ potential surface.

The aim of our double-photoionization (DPI) study of CH_4 is twofold. Firstly, by measuring the absolute DPI cross section as a function of the excitation energy we obtain information on electron correlation effects occurring in the DPI of CH_4. Secondly, by determining both the initial and the final states of CH_4^{2+} dissociation processes, we achieve a state-to-state study of CH_4^{2+} dissociation. Our results will be compared with those of existing calculations on the extent of the stability of the CH_4^{2+} cation.

II. EXPERIMENTAL

The principle of our photoion-photoion coincidence (PIPICO) method[1] is to detect, with a single detector, both ionic fragments issuing from the dissociation of a doubly charged cation M^{2+}, and to measure by delayed coincidences the difference between their times of flight. These measurements are then repeated at different excitation energies. From a comparison of the experimental photoion-photoion coincidence curve with a simulated one, fragment ions can be identified and their kinetic energy determined. The results also enable us to determine the ionization energies of dissociative states of M^{2+} and the absolute double-photoionization cross section as a function of the excitation energy.

The experimental setup was described in Ref. 1. Briefly, synchrotron radiation from ACO (les Anneaux de Collisions d'Orsay), dispersed by a McPherson 1 m normal incidence grating (3600 lines/mm, blazed at 400 Å) is focused on the photoionization region of the PIPICO apparatus (Fig. 1). The bandpass was $\cong 0.1$ Å over the excitation range 354—238 Å (35—52 eV). The photon intensity at 400 Å was $\cong 5\times10^8$ photons s^{-1} $Å^{-1}$. CH_4 molecules (Air Liquide gas product) are introduced through a hypodermic syringe needle into the ionization region at a pressure $\cong 10^{-4}$ Torr. The needle is far enough from the photon-beam axis ($0y$ in Fig. 1) so that one can consider the pressure to be uniform within the parallelepiped shown in Fig. 1. This parallelepiped, which represents the shape of the photon beam in the region where photoions are extracted, has the dimensions, 1 mm × 15 mm × 3 mm along the **x**, **y**, and **z** axes, respectively. We will assume, in the following, that CH_4^{2+} doubly charged cations are produced (by double photoionization of neutral CH_4 molecules) uniformly throughout the parallelepiped in Fig. 1. However, the results obtained are believed not to depend strongly on the exact distribution of CH_4^{2+} cations produced in this volume (see later).

It will be shown to be consistent with experimental results to assume that the dissociation processes observed are so rapid that the ionic fragments A^+ and B^+ originating from CH_4^{2+} are produced at the same place as the parent CH_4^{2+} cation. Fragments A^+ and B^+ have total times of flight t_{A+} and t_{B+}, respectively, for travel-

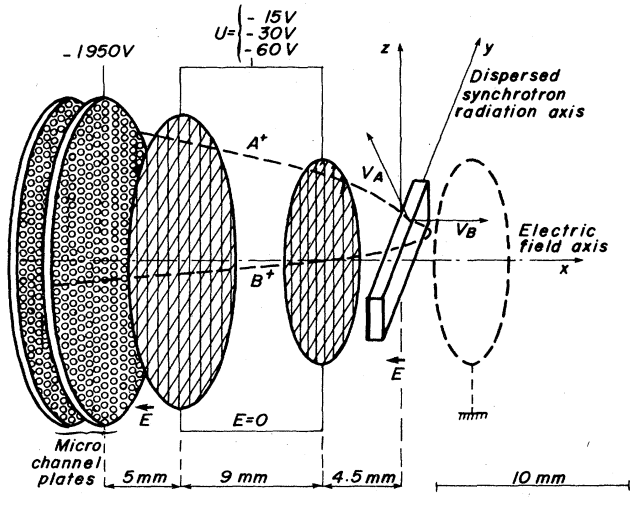

FIG. 1. Schematic diagram of the photoion-photoion coincidence (PIPICO) apparatus. $\mathbf{v}_A$ and $\mathbf{v}_B$ are initial velocity vectors of the fragments A^+ and B^+ produced by the dissociation of doubly charged cations.

ing through the first low-electric-field region (15 V/cm $< E <$ 60 V/cm), then through the field-free region ($E=0$), and finally through the strong-electric-field region (3780 V/cm $< E <$ 3870 V/cm). The difference of times of flight $\Delta t = t_{A^+} - t_{B^+}$ is recorded by sending the pulses from the ion detector into both the start and the stop input of a time-to-amplitude coverter (TAC). The start input signal was delayed to avoid the TAC starting and stopping with the same pulse. Coincidence recording and time calibrations are described in Ref. 1. Typical PIPICO curves are shown in Figs. 3, 4, and 5. They represent the number of coincidences detected as a function of Δt. For each PIPICO curve, various Δt values correspond to various orientations of the initial velocity vector of each fragment (see Fig. 1).

As mentioned above, identification of the fragments and determination of their kinetic energy are made by comparison between experimental and simulated PIPICO curves. We will now discuss the simulation procedure.

A. Simulation of the PIPICO curves

We consider two ionic fragments A^+ and B^+ emitted with velocity vectors $\mathbf{v}_A$ and $\mathbf{v}_B$ from a point M_0 $(\mathbf{x}_0,\mathbf{y}_0,\mathbf{z}_0)$ located inside the parallelepiped mentioned above (see also Fig. 1). In the $\mathbf{x},\mathbf{y},\mathbf{z}$ system of axes, the latitude and longitude angles of $\mathbf{v}_A$ are θ and ϕ, respectively (Fig. 2). A second $\mathbf{x}',\mathbf{y}',\mathbf{z}'$ reference system is used whose $\mathbf{z}'$ axis is along $\mathbf{v}_A$ and whose $\mathbf{x}'$ axis is in the $\mathbf{xy}$ plane. The latitude and longitude angles of $\mathbf{v}_B$ are then θ' and ϕ', respectively, in this latter reference system.

In the simplest case, when the doubly charged parent cation dissociates into only two ionic fragments A^+ and B^+, with masses m_A and m_B, respectively, one has $\theta'=\pi$ and ϕ' no longer has to be considered. In this case the total kinetic energy E_{kin} released in the dissociation is given by

$$E_{\text{kin}} = \tfrac{1}{2} m_A \mathbf{v}_A^2 (1 + m_A/m_B) = \tfrac{1}{2} m_B \mathbf{v}_B^2 (1 + m_B/m_A) .$$

In the case of dissociation into two ionic fragments A^+ and B^+ plus some other neutral fragment(s), θ', ϕ', $|\mathbf{v}_A|$, and $|\mathbf{v}_B|$ can each have a range of values for a given kinetic energy released. In order to simplify our calculations we will only consider in the following some dissociation models (statistical or impulsive models) which enable us to calculate θ', $|\mathbf{v}_A|$, and $|\mathbf{v}_B|$ as unequivocal functions of m_A, m_B, and E_{kin}.

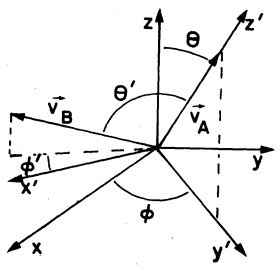

FIG. 2. Spherical coordinates of $\mathbf{v}_A$ and $\mathbf{v}_B$, respectively, in the $\mathbf{x},\mathbf{y},\mathbf{z}$ and $\mathbf{x}',\mathbf{y}',\mathbf{z}'$ systems of axes.

For a particular dissociation process and a given dissociation model with a fixed total kinetic energy, we can calculate the time needed for each ionic fragment (A^+ and B^+) to reach the ion detector. In order to be detected, fragments have to traverse the first mesh (15 mm diameter), then through the second mesh (21 mm diameter), and then strike the 23.3 mm diameter sensitive surface of the first multichannel plate. Only those events for which both A^+ and B^+ reach the ion detector are counted as coincidences. The difference of times of flight $\Delta t = t_{A^+} - t_{B^+}$ is then divided by the time interval per channel to give the corresponding channel number. The content of this channel is incremented by the product of $\sin\theta$ with the normalization factor $\frac{1}{2}\pi$. $\sin\theta$ is proportional to the probability $(\sin\theta\, d\theta\, d\phi)/4\pi$ for the fragment A^+ to be ejected with latitude and longitude angles, respectively, between θ and $\theta + d\theta$, and ϕ and and $\phi + d\phi$. This procedure is repeated for many random values of $\mathbf{x}_0,\mathbf{y}_0,\mathbf{z}_0$ (within the limits of the parallelepiped of Fig. 1), θ, ϕ, and ϕ' until the simulated coincidence curve represents good statistical behavior. Each simulated PIPICO curve corresponds to at least 9000 different trajectories of the fragments; each curve was normalized to the maximum of the corresponding experimental curve.

We report in Fig. 3 the experimental PIPICO curve (curve a) obtained at the excitation energy of 38.5 eV, together with the simulated curves (curves b–e) corresponding to the following four dissociation processes:

$$CH_4^{2+} \rightarrow CH_3^+ + H^+, \quad \text{with } E_{\text{kin}} = 5.3 \text{ eV} \tag{1}$$

$$CH_4^{2+} \rightarrow CH_2^+ + H_2^+, \quad \text{with } E_{\text{kin}} = 5.3 \text{ eV} \tag{2}$$

$$CH_4^{2+} \rightarrow CH_2^+ + H^+ + H, \quad \text{with } E_{\text{kin}} = 5 \text{ eV}, \quad \theta' = 180°, \; E_{\text{kin}}(H) = 0 \tag{3}$$

$$CH_4^{2+} \rightarrow CH^+ + H^+ + H_2, \quad E_{\text{kin}} = 5 \text{ eV}, \quad \theta' = 180°, \; E_{\text{kin}}(H_2) = 0 . \tag{4}$$

The particular conditions retained for reactions (3) and (4) will be discussed later. Other dissociation processes energetically accessible (see Table IV) were also considered and were found to be incompatible with our experimental data. For each PIPICO curve we define the $\Delta t_{\max}$ and $\Delta t_{\min}$ as those values which correspond to the maximum and minimum values of $\Delta t = t_{A^+} - t_{B^+}$ with nonzero coincidences. We note that $(\Delta t_{\max} + \Delta t_{\min})/2$ is constant for a given dissociation process whatever the total kinetic energy or the θ' angle in processes (3) and (4). Only the difference $\Delta t_{\max} - \Delta t_{\min}$ depends on E_{kin} and θ'. It is clear from Fig. 3 that the dissociation process observed at 38.5-eV excitation energy corresponds to the $CH_4^{2+} \rightarrow CH_3^+ + H^+$ process and cannot correspond to processes (2), (3), or (4) irrespective of the E_{kin} and θ' values involved in these processes. The simulated PIPICO curves were obtained by assuming an isotropic fragmentation of CH_4^{2+}. The excellent agreement between the experimental (curve a of Fig. 3) and the simulated (curve b of Fig. 3) PIPICO curve indicates that under our experimental conditions the dissociation is indeed isotropic. We remark

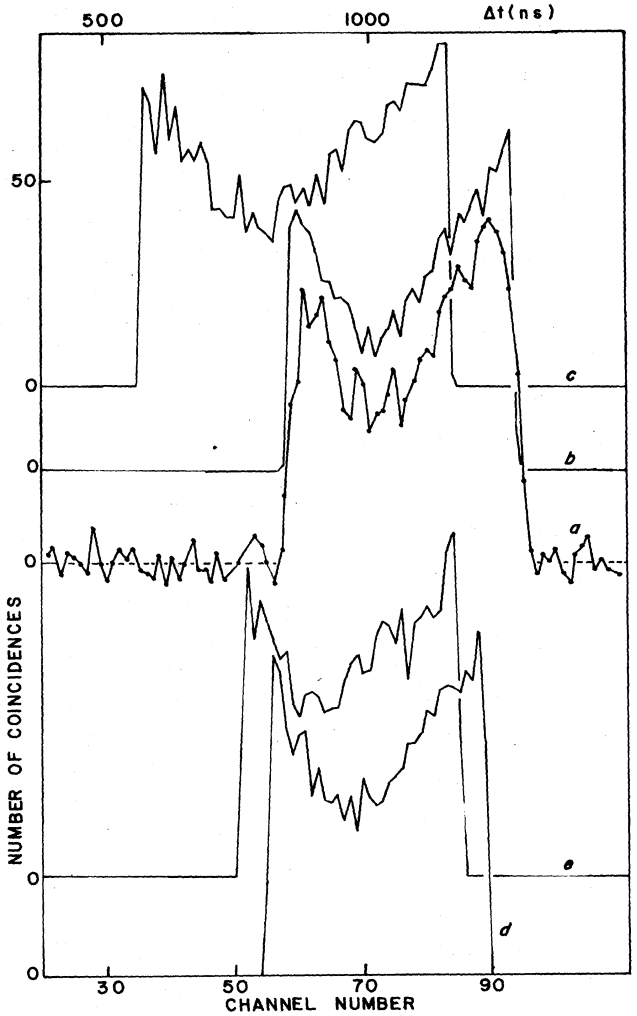

FIG. 3. Comparison of experimental and simulated PIPICO curves. The experimental PIPICO curve (a) was recorded at a photon excitation energy of 38.5 eV. Extraction electric field is 30 V/cm. Ion count rate is approximately 1000/s. Time of accumulation is 3 h. Curves b, c, d, and e are simulated PIPICO curves corresponding to processes 1, 2, 3, and 4, respectively (see text).

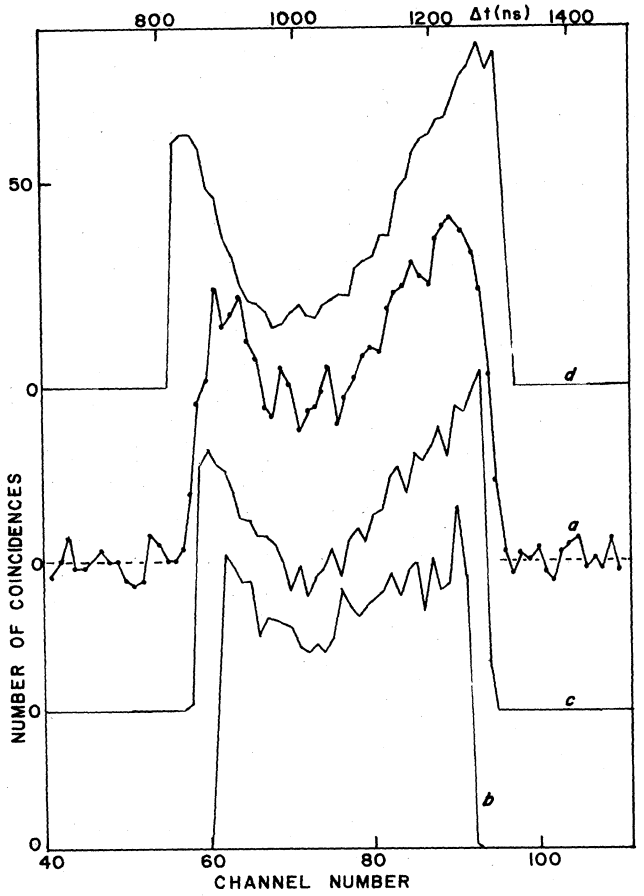

FIG. 4. Comparison of experimental (a) with simulated (b,c,d) PIPICO curves. The experimental curve (a) is the same as that in Fig. 3 and corresponds to a 38.5 eV photon excitation energy. Extraction electric field is 30 V/cm. Simulated curves b, c, and d correspond to the $CH_4^{2+} \rightarrow CH_3^+ + H^+$ process with a total kinetic energy released of 4, 5.3, and 7 eV, respectively.

that in both the a and b curves the local maximum in the Δt_{min} region is much lower than the maximum in the Δt_{max} region. This is due to the fact that Δt and θ are not linearly related. We also remark that curves a and b of Fig. 3 are depressed in the middle. We verified, with the simulated curve, that this is due to angular discrimination of the collection efficiency for high kinetic-energy ionic fragments.

Figure 4 shows how comparison of the experimental PIPICO curve with curves simulated for various values of E_{kin} enables measurement to be made of the total kinetic energy E_{kin} released. We remark that the $\Delta t_{max} - \Delta t_{min}$ value (width of the PIPICO curve) and the depth of the depression due to angular discrimination both vary with E_{kin}.

Looking at Fig. 4, we note that simulated curve 4c, which best fits the experimental curve, rises abruptly at Δt_{max} and Δt_{min} values of Δt, whereas the experimental curve 4a rises much less sharply in these regions. As will be discussed in Sec. III C 1, this is probably due to the distribution, around the 5.3-eV value, of the total kinetic energy released.

In order to check the validity of our method, we also recorded some PIPICO curves for various values of the extracting electric field. The PIPICO curve recorded using a 15-V/cm electric field is shown in curve a of Fig. 5 together with the simulated curve (curve b) corresponding to the $CH_4^{2+} \rightarrow CH_3^+ + H^+$ process. A similar comparison can be made between experimental (curve c of Fig. 5) and simulated (curve d of Fig. 5) curves, but for a 60-V/cm extraction electric field. We see that the angular discrimination in our PIPICO system is strong for a 15-V/cm extraction field and much smaller for a 60-V/cm electric field. We also remark that simulation of the experimental PIPICO curves is quite good in each case (Figs. 3, 4, and 5).

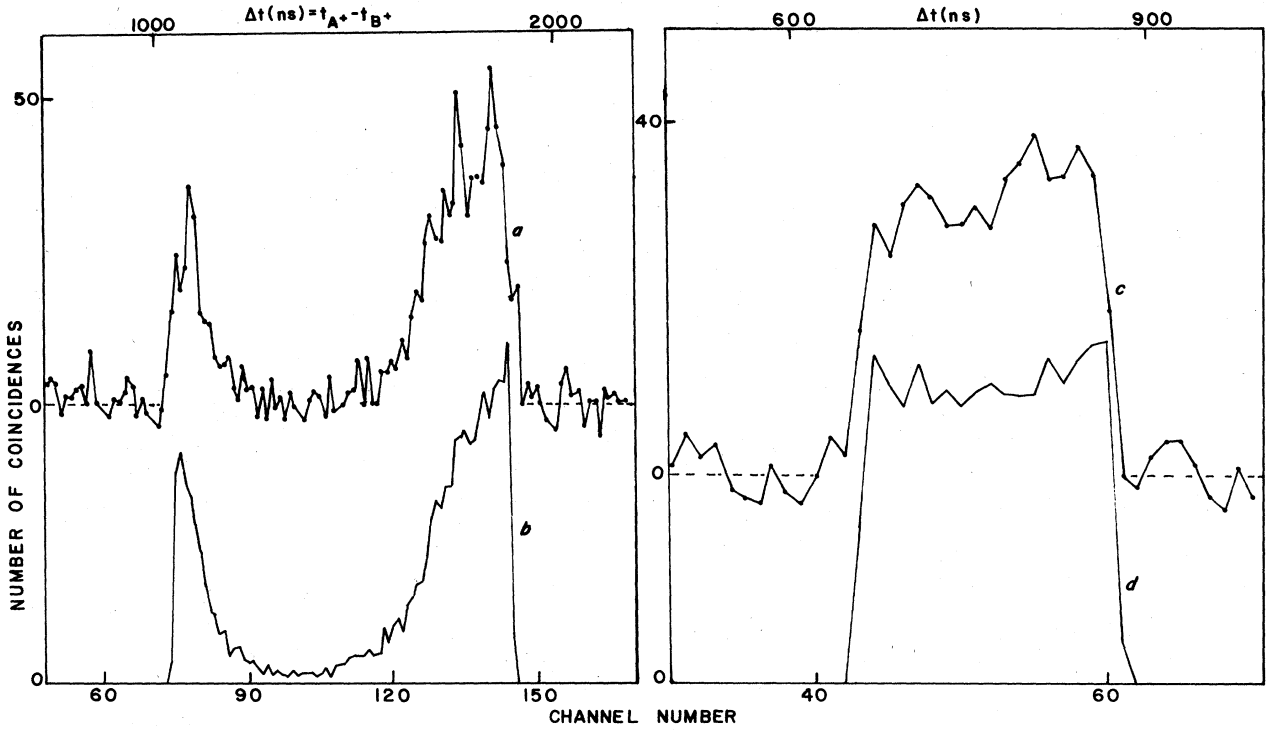

FIG. 5. The experimental PIPICO curve (a), at 38 eV photon excitation energy (ion count rate is 1000/s; time of accumulation is 2.2 h), and the simulated curve (b) corresponding to the $CH_4^{2+} \rightarrow CH_3^+ + H^+$ process with $E_{kin} = 5.3$ eV, were obtained with a 15-V/cm electric field for extraction of ions. The experimental PIPICO curve (c), at a 37-eV photon excitation energy (ion count rate is 1000/s; time of accumulation is 1 h), and the simulated curve (d) corresponding to the $CH_4^{2+} \rightarrow CH_3^+ + H^+$ process with $E_{kin} = 5.3$ eV were obtained with a 60-V/cm electric field for extraction of ions.

B. Determination of the double-photoionization cross sections

The double-photoionization cross section $\sigma^{2+}(E)$ was obtained as a function of the photon excitation energy E from the following relation:[1]

$$\frac{\sigma^{2+}(E)}{\sigma_i(E)+\sigma^{2+}(E)} = \frac{N_c}{N_i f_i} . \tag{5}$$

From this relation we deduce an expression for $\sigma^{2+}(E)$ relative to the total ionization cross section $\sigma_i(E)$,

$$\frac{\sigma^{2+}(E)}{\sigma_i(E)} = \frac{N_c}{N_i f_i} \frac{1}{\left[1-\dfrac{N_c}{N_i f_i}\right]} \tag{6}$$

and for $\sigma^{2+}(E)$ relative to the single-photoionization cross section $\sigma^{+}(E)$,

$$\frac{\sigma^{2+}(E)}{\sigma^{+}(E)} = \frac{N_c}{N_i f_i} \frac{1}{\left[1-\dfrac{2N_c}{N_i f_i}\right]} . \tag{7}$$

N_c and N_i are, respectively, the total number of coincidences and the total number of ions detected. N_i is measured directly with an ion counter. N_c is obtained by integrating the experimental PIPICO curve over Δt. We checked, by appropriate calibrations using SO_2 and CH_4, that the ion detection efficiency f_i was equal to 0.29 as in our earlier work.[1]

We determined N_c/N_i from the 60-V/cm electric field experiments in order to avoid undesirable angular discrimination effects. However, even with this high ion extraction field, angular discrimination is not completely negligible. By simulating the PIPICO curves of the $CH_4^{2+} \rightarrow CH_3^+ + H^+$ ($E_{kin} = 5.3$ eV) process, both with and without angular discrimination, we obtained N_c (no discrimination)/N_c (discrimination) = 1.21. We also simulated N_i, the total number of ions detected, both with and without angular discrimination. At a 39-eV excitation energy we calculated that N_i (no discrimination)/N_i (discrimination) = 1.03. This result was obtained using literature data[14,23–26] on the percentages of all ionic fragments produced by excitation of CH_4 at 39 eV, together with their kinetic energies. We considered that the variation of the "discrimination ratios" with excitation energy is negligible. Thus, to take into account angular-discrimination effects, we multiplied the experimental N_c/N_i ratio (obtained with discrimination) by the 1.18 factor (i.e., by the ratio of the two discrimination ratios).

III. RESULTS AND DISCUSSION

A. Double-photoionization cross sections

The cross section $[\sigma^{2+}(E)]$ for double photoionization (DPI) of CH_4, relative to the single-photoionization cross

TABLE I. Double-photoionization cross section $[\sigma^{2+}(E)]$ relative to the single-photoionization cross section $[\sigma^{+}(E)]$ as a function of the excitation photon energy E.

E (eV)	σ^{2+}/σ^{+}
35.3	$(8.1 \pm 4.9) \times 10^{-5}$
35.5	$(1.8 \pm 0.6) \times 10^{-4}$
36	$(2.5 \pm 0.8) \times 10^{-4}$
36.5	$(4.2 \pm 1.2) \times 10^{-4}$
37	$(6.1 \pm 0.6) \times 10^{-4}$
37.5	$(9.4 \pm 1.3) \times 10^{-4}$
38	$(1.44 \pm 0.04) \times 10^{-3}$
38.25	$(1.6 \pm 0.1) \times 10^{-3}$
38.5	$(1.97 \pm 0.08) \times 10^{-3}$
38.75	$(2.36 \pm 0.14) \times 10^{-3}$
39	$(2.9 \pm 0.1) \times 10^{-3}$
39.25	$(3.16 \pm 0.17) \times 10^{-3}$
39.5	$(3.93 \pm 0.09) \times 10^{-3}$
40	$(4.7 \pm 0.2) \times 10^{-3}$
40.5	$(6.0 \pm 0.3) \times 10^{-3}$
41	$(7.1 \pm 0.4) \times 10^{-3}$
41.5	$(7.7 \pm 0.4) \times 10^{-3}$
42	$(8.9 \pm 0.2) \times 10^{-3}$
43	$(1.02 \pm 0.06) \times 10^{-2}$
44	$(1.24 \pm 0.08) \times 10^{-2}$
45	$(1.34 \pm 0.08) \times 10^{-2}$
46	$(1.42 \pm 0.08) \times 10^{-2}$
47	$(1.44 \pm 0.08) \times 10^{-2}$
48	$(1.30 \pm 0.08) \times 10^{-2}$
49	$(1.15 \pm 0.07) \times 10^{-2}$
50	$(1.03 \pm 0.06) \times 10^{-2}$
51	$(9.3 \pm 0.6) \times 10^{-3}$
52	$(9.0 \pm 0.9) \times 10^{-3}$

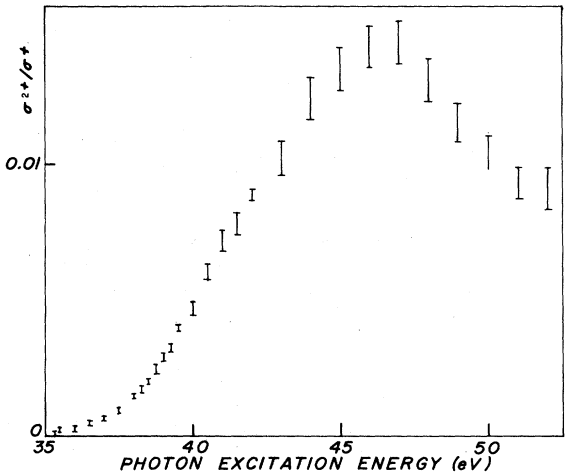

FIG. 6. Measured ratio of double- to single-photoionization cross sections of CH_4.

section $[\sigma^{+}(E)]$, as obtained from relation (7), is given in Table I and shown in Fig. 6 as a function of photon excitation energy E. Absolute double-photoionization (DPI) cross sections reported in Fig. 7 were calculated from relation (6). The σ_i values used in this calculation were taken as being equal to the absorption cross sections measured by Lee *et al.*,[27] by assuming that at these energies the ionization efficiency[28] is unity. We will now consider two aspects of Figs. 6 and 7.

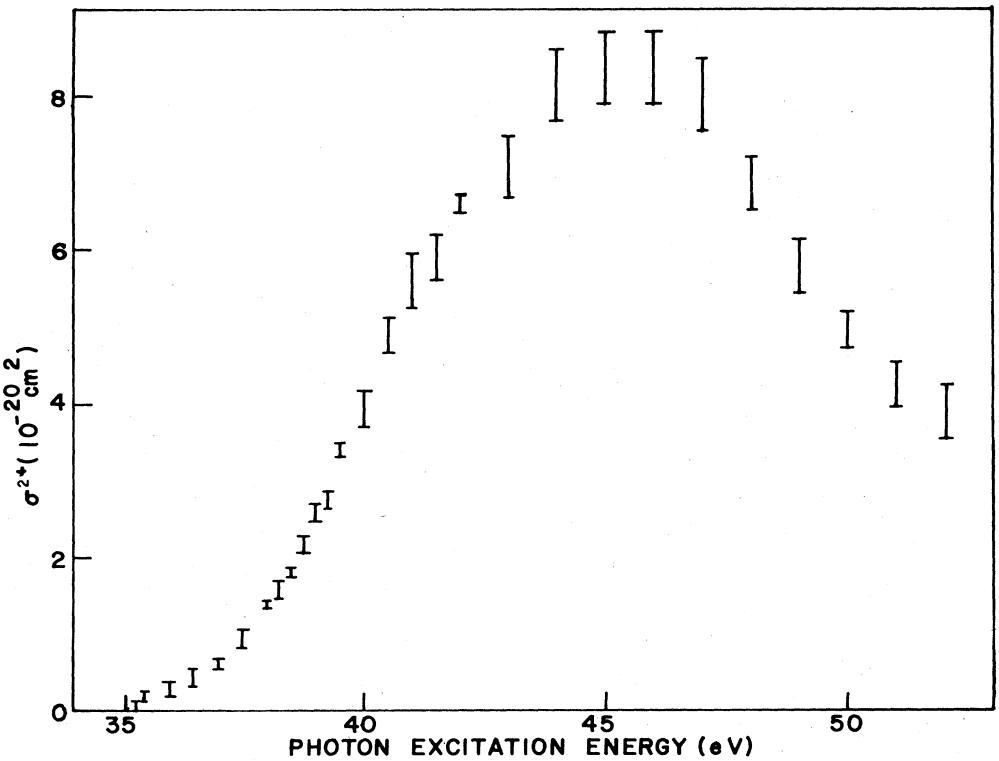

FIG. 7. Measured absolute double-photoionization cross section of CH_4 over the photon excitation-energy range 35—52 eV.

TABLE II. Maximum or asymptotic values of the σ^{2+}/σ^{+} ratio and of the absolute σ^{2+} cross section in the outer-shell energy region for Ne, CO_2, SO_2, and CH_4.

Atom or molecule	$\left(\frac{\sigma^{2+}}{\sigma^{+}}\right)_{max}$	$(\sigma^{2+})_{max}$ (10^{-20} cm^2)
Ne (Ref. 30)	0.12	25
CO_2 (Refs. 27, 29)	0.025	35
SO_2 (Ref. 1)	0.030	19
CH_4 (this work)	0.014	8.4

(i) We remark that the σ^{2+}/σ^{+} ratio and σ^{2+} values are smaller, throughout the 35—52-eV energy range, as compared to known values for other molecules and for the isoelectronic neon atom (see Table II). The $(\sigma^{2+}/\sigma^{+})_{max}$ and $(\sigma^{2+})_{max}$ values in Table II occur in the low-energy region where direct DPI processes dominate. These values could possibly increase at higher energies because of the occurrence of Auger processes. We emphasize here that, except for neon, it is not certain that σ^{2+} is the true total cross section for DPI since in some experiments[29] only undissociated metastable doubly ionized species are detected, whereas in other cases[1] only some of the dissociative doubly ionized states are counted. Since no (CH_4^{2+}) metastable states are formed by electron impact, they are not expected to be produced by DPI of CH_4. The low values of σ^{2+}/σ^{+} and σ^{2+} for CH_4, as compared to CO_2 and SO_2, may be related to the general trend observed in rare-gas studies[30,31] where the asymptotic value of the ratio of double to single photoionization decreases from Ar to He with decreasing principal quantum number of the ejected electrons. The smaller DPI cross sections in CH_4 as compared to the isoelectronic neon atom may be due to fewer many-particle interactions in CH_4 because of larger volume.

(ii) The σ^{2+}/σ^{+} curve in Fig. 6 passes through a maximum at about 47 eV and then decreases at higher energies. The possibility of having a maximum in the double to single ionization ratio was discussed in the case of He by Carlson[32] and by Van der Wiel and Wieber[33] in the case of He, Ne, and Ar. However, no experimental maximum is evident in the numerous studies of rare gases.[30—32,34] In the molecular case of SO_2 (Ref. 1) also, no maximum was observed in the σ^{2+}/σ^{+} curve. The exact origin of the maximum in the CH_4 case is difficult to elucidate in the absence of a reliable model for molecular DPI calculations. We note that, if present in our experiment, some light of low energy ($E > 13.6$ eV) scattered by the monochromator could also account for such a maximum since it would decrease σ^{2+}/σ^{+} at higher energies where the transmission of the monochromator is low. Though it is difficult to completely rule out this possibility we remark that among all the molecular systems that we studied [SO_2 (Ref. 1), CO_2 (Ref. 35), and NH_3 (Ref. 35)], CH_4 is the only case where a maximum of the σ^{2+}/σ^{+} curve was observed in the 30—52-eV energy range.

B. Electronic states of CH_4^{2+}

The low energy part of the σ^{2+} curve is shown in more detail in Fig. 8. As for the case of single ionization by electron impact, the threshold law for double photoionization (DPI) was predicted by Wannier[36] to be approximately linear with energy. Such behavior was indeed observed for the DPI of SO_2 (Ref. 1). We fitted the σ^{2+} curve in Fig. 8 to linear segments, in similar fashion to the treatment of single ionization by electron impact.[37,38] The breaks in the curve are generally believed to correspond to the opening of new ionization channels. Three breaks, at 35.0, 37.15, and 38.5 eV, respectively, are indicated in Fig. 8. However, no important change in the form of the PIPICO curves was discernable over the 35.3—38.5-eV excitation-energy range. In this range all the PIPICO curves look like those of Fig. 3, curve *a* (30 V/cm), 5, curve *a* (15 V/cm), and 5, curve *c* (60 V/cm). It is thus improbable that the inflection at 37.15 eV corresponds to the opening of a new DPI channel. On the other hand, for energies greater than 38.5 eV the PIPICO curves are markedly different from those at lower energy (see Sec. III C), indicating that a new DPI channel opens up at 38.5 eV. We then conclude from the PIPICO results that two different DPI channels have onset energies at, respectively, 35.0 and 38.5 eV.

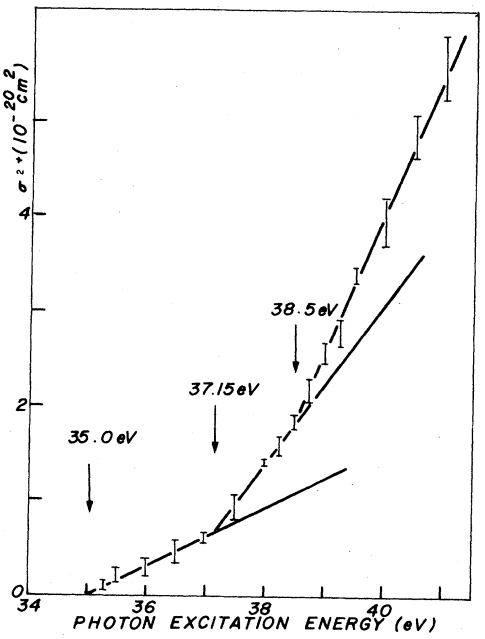

FIG. 8. Measured absolute double-photoionization cross section of CH_4 over the photon excitation-energy range 35—41 eV. Arrows indicate the breaks in the curve fitted to linear segments.

The lowest electronic states of CH_4^{2+} are produced by removing two electrons from the $1t_2$ orbital. This gives rise to a multiplet of CH_4^{2+} states: $^3T_1$, ^1E, $^1T_2$, and $^1A_1$. Their vertical energies have been calculated (see Table III) using both Hartree-Fock and multiconfiguration models. Comparison of these calculated energies with our PIPICO results leads to the following remarks: (i) The first CH_4^{2+} channel, whose experimental onset energy is at 35.0 eV, may be assigned to the $^3T_1$ state. We note that the break at 37.15 eV in the σ^{2+} curve coincides with the calculated vertical energies (Table III) of this state. (ii) The second

TABLE III. Calculated (vertical) and experimental (threshold) energies (eV) of the CH_4^{2+} states obtained by removing two electrons from the $1t_2$ orbital.

CH_4^{2+} state	HF calculation (Ref. 16)	HF calculation (Ref. 17)	MCSCF calculation (Ref. 21)	Experimental (this work)
$^3T_1$	36.32	37.13	36.9	35.0
^1E	38.80	38.17		38.5
$^1T_2$	39.11	40.11		
$^1A_1$		42.57		

CH_4^{2+} channel, whose experimental onset energy is at 38.5 eV is assigned to the ^1E state. In this case the onset energy is very near to the calculated vertical energy (Table III).

When the onset energy is close to the vertical energy (i.e., narrow Franck-Condon energy region of the potential energy surface), it is expected that the convolution of Franck-Condon factors with the linearly increasing electronic part of σ^{2+} gives a linear threshold law of σ^{2+}, as observed in Fig. 8 for energies above the onset of the ^1E state at 38.5 eV. On the other hand, when the onset energy is much lower than the vertical energy (i.e., broad Franck-Condon energy region of the potential surface), the convolution product can lead to a nonlinear variation of σ^{2+}. This could explain that the σ^{2+} curve of Fig. 8 cannot be fitted by a single linear segment in the energy region (35.0—38.5 eV) of the $^3T_1$ state, and that we observe a break at the 37.15-eV vertical energy of this state. From a multiconfiguration self-consistent-field (MCSCF) calculation, Siegbahn[21] found the energy of the CH_4^{2+} ($^3T_1$) state to be 36.9 and 35.2 eV at the respective r(C—H) distances of 1.092 and 1.288 Å. We calculated that the $v=0$ turning point[39] of the $CH_4(\tilde{X}\,^1A_1)$ potential surface is at an r(C—H) distance of 1.028 Å. We thus estimate, within a linear approximation (see Fig. 9), the onset energy of the $CH_4^{2+}(^3T_1)$ state, along the r(C—H) coordinate to be at 35.9 eV. Taking into consideration other coordinates, in particular the bond angles, could lower this energy. Thus the experimental value of 35.0 eV is well compatible with the estimated onset energy of the $^3T_1$ state of CH_4^{2+}.

Although it has not been specified that the $CH_4^{2+}(^3T_1)$ state is populated in the Auger[6] and the double-charge-transfer (DCT)[15] experiments, the broad band extending down to 36—37 eV observed in both of these experiments, lends some credence to the idea that this state is indeed populated. The fact that the Franck-Condon region of the $^3T_1$ state is very broad, as observed in the PIPICO experiment, could explain that this state could not be resolved in the Auger and DCT experiments.

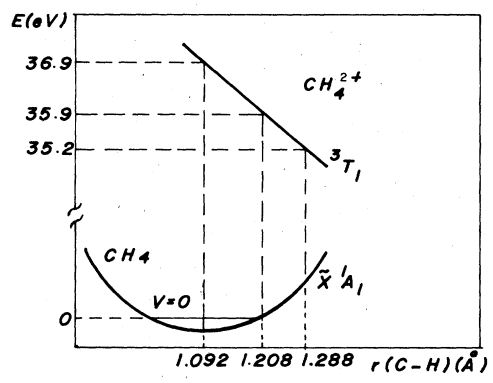

FIG. 9. Sections of the $CH_4(\tilde{X}\,^1A_1)$ and $CH_4^{2+}(^3T_1)$ potential-energy surfaces.

In the case of neon ($1s^22s^22p^6$), the removal of two electrons from the $2p$ orbital gives rise to a multiplet of ^3P (corresponding to the $^3T_1$ state of CH_4^{2+}), ^1D (^1E,$^1T_2$), and ^1S ($^1A_1$) states. We remark that the lower electronic states of Ne^{2+} (or other rare gases) produced by double photoionization (DPI) have not been identified,[30,31] so that a comparison between CH_4^{2+} states and those of the isoelectronic Ne^{2+} atom produced by DPI is not possible. Although electron-impact excitation processes differ from photon-impact processes, we remark, however, that all three states, ^3P, ^1D, and ^1S, were observed in the first differential ionization curve of double ionization of Ne by electron impact.[40]

To sum up, we consider that both triplet ($^3T_1$) and singlet (^1E) states of CH_4^{2+} are observed in the DPI of methane. Furthermore, as can be seen from Figs. 7 and 8, the cross section for formation of the triplet state is an important part of the total DPI cross section. This shows that, in this case, spin-conservation selection rules are weak for double photoionization. As noted by Kelly,[41] one would think *a priori* that the correlation energy is less important for two electrons with parallel spins. The large amount of triplet state produced in DPI of methane would then indicate that in this case, the correlation energy of the two ejected electrons is not the dominant parameter to explain the DPI results.

C. Dissociation of CH_4^{2+}

Some of the numerous possible dissociation channels of the doubly charged CH_4^{2+} cation are indicated in Table IV. We considered fragmentations of CH_4^{2+} into two fragments as well as into three, four, and five products. The dissociation of molecular species into more than two fragments has rarely been studied.[47] However, we believe that such processes are favored in doubly charged cations as compared to neutral or singly charged molecules for the following reasons: (i) the threshold energy for dissociation into three fragments can be below the lowest vertical double-ionization energy; (ii) because of Coulomb interaction between positive charges, the repulsive forces tend to dissociate the molecule into several products.

TABLE IV. Threshold energies for formation of various products from CH_4^{2+} calculated with respect to the vibrationless level of the $\tilde{X}\,^1A_1$ ground state of CH_4.

	Electronic states of products	Energy (eV)	References
2 fragments			
$CH_4 \rightarrow CH_3^+ + H^+$	$\tilde{X}\,^1A_1',(^1S)$	27.8	39,42
	$\tilde{a}\,^3E',(^1S)$	32.7	
	$\tilde{A}\,^1E',(^1S)$	34.1	
	$\tilde{b}\,^3A_2'',(^1S)$	40.5	
$CH_4 \rightarrow CH^+ + H_3^+$	$X^1\Sigma^+,\tilde{X}\,^1A_1$	28.4	21
$CH_4 \rightarrow CH_2^+ + H_2^+$	$\tilde{X}\,^2A_1,X^2\Sigma_g^+$	30.5	25,39
3 fragments			
$CH_4 \rightarrow CH_2^+ + H^+ + H$	$\tilde{X}\,^2A_1,(^1S),^2S$	33.3	26,39,43,44
	$\tilde{A}\,^2B_1,(^1S),^2S$	35	
$CH_4 \rightarrow CH^+ + H^+ + H_2$	$X^1\Sigma^+,(^1S),X^1\Sigma_g^+$	33.4	26,39,45
$CH_4 \rightarrow C^+ + H_2^+ + H_2$	$^2P,X^2\Sigma_g^+,X^1\Sigma_g^+$	34.5	21
$CH_4 \rightarrow C + H^+ + H_3^+$	$^3P,(^1S),\tilde{X}\,^1A_1$	34.8	21,45
$CH_4 \rightarrow CH^+ + H_2^+ + H$	$X^1\Sigma^+,X^2\Sigma_g^+,^2S$	35.2	26,39,45
$CH_4 \rightarrow CH_2 + H^+ + H^+$	$\tilde{X}\,^3B_1,(^1S),(^1S)$	36.5	26,39
$CH_4 \rightarrow CH + H^+ + H_2^+$	$X^2\Pi,(^1S),X^2\Sigma_g^+$	38.2	26,39,45
$CH_4 \rightarrow C + H_2^+ + H_2^+$	$^3P,X^2\Sigma_g^+,X^2\Sigma_g^+$	38.7	21,45
4 fragments			
$CH_4 \rightarrow C^+ + H^+ + H + H_2$	$^2P,(^1S),^2S,X^1\Sigma_g$	37.5	26,39,45,46
$CH_4 \rightarrow CH^+ + H^+ + H + H$	$X^1\Sigma^+,(^1S),^2S,^2S$	37.9	
$CH_4 \rightarrow C^+ + H_2^+ + H + H$	$^2P,X^2\Sigma_g^+,^2S,^2S$	39.3	
$CH_4 \rightarrow C + H_2 + H^+ + H^+$	$^3P,X^1\Sigma_g^+,(^1S),(^1S)$	39.8	
$CH_4 \rightarrow CH + H + H^+ + H^+$	$X^2\Pi,^2S,(^1S),(^1S)$	40.9	
$CH_4 \rightarrow C + H + H^+ + H_2^+$	$^3P,^2S,(^1S),X^2\Sigma_g^+$	41.6	
5 fragments			
$CH_4 \rightarrow C^+ + H^+ + H + H + H$	$^2P,(^1S),^2S,^2S,^2S$	42.0	
$CH_4 \rightarrow C + H^+ + H^+ + H + H$	$^3P,(^1S),(^1S),^2S,^2S$	44.4	
Doubly charged fragments			
$CH_4 \rightarrow CH_3^{2+} + H$	$\tilde{X}\,^2A_1,^2S$	33.3	39,21
		37.4	39,22
$CH_4 \rightarrow CH_2^{2+} + H_2$	$X^1\Sigma_g^+,X^1\Sigma_g^+$	34.7	39,21
		36.0	39,22
$CH_4 \rightarrow CH_2^{2+} + H + H$	$X^1\Sigma_g^+,^2S,^2S$	39.2	39,21
		40.5	39,22
$CH_4 \rightarrow C^{2+} + H_2 + H_2$	$^1S,X^1\Sigma_g^+,X^1\Sigma_g^+$	43.3	21

Although doubly charged fragments resulting from a doubly charged parent ion cannot be detected by the PIPICO method, we also mention in Table IV some processes involving these species. The threshold energies for formation of the various products were calculated from the literature values of ionization and dissociation energies (see references in Table IV). Except for the two dissociation channels which will be discussed in detail in the following, we only considered stable products in their ground electronic states.

Little information on the dissociation of CH_4^{2+} is available in the literature. It is known[13,14] that high kinetic-energy electron impact on CH_4 produces doubly charged CH_4^{2+} cations which dissociate into various pairs of ions. The most abundant pairs (relative abundance in parentheses) obtained with 10-keV electron impact[14] are $H^+ + CH_3^+$ (1), $H^+ + CH_2^+$ (1.42), $H^+ + CH^+$ (0.97), $H^+ + C^+$ (0.64), and $H_2^+ + CH_2^+$ (0.32). However, we do not know the kinetic energy of these fragments, neither do we know the CH_4^{2+} electronic states involved and the processes of their formation. We note in particular that at such a high (10-keV electron impact) excitation energy, the double ionization of CH_4 may be dominated by carbon $1s$ ionization[8] followed by Auger processes. It follows that with 10-keV electron impact, the CH_4^{2+} states populated and the corresponding dissociation products may be different from those occurring in double photoionization so that a direct comparison between the two sets of results is difficult. Some other dissociation processes were observed in the charge-stripping experiment:[19] (i) dissociation of CH_4^{2+} into CH_2^{2+} plus some neutral products; (ii) dissociation of CH_4^+ into C^{2+} plus some neutral products

(see Table IV); (iii) a slow $CH_4^{2+} \rightarrow CH_3^+ + H^+$ dissociation with a 5.5±0.5-eV kinetic-energy release. As noted by several authors,[19–21] and discussed earlier here, the charge-stripping experiment produces CH_4^{2+} cations which may have a geometry very different from that obtained by other methods (electron impact, double photoionization) where ionization corresponds to vertical (Franck-Condon) transitions from the neutral CH_4 molecule. It follows that charge-stripping results may differ significantly from those of electron impact or DPI experiments.

We will now consider separately the dissociation of CH_4^{2+} in the two electronic states populated by double photoionization as discussed in Sec. III B.

1. Dissociation of CH_4^{2+} in its $^3T_1$ state

Some of the PIPICO curves corresponding to the dissociation of the $^3T_1$ state are shown in curve *a* of Fig. 3, curve *a* of Fig. 4, and curves *a* and *c* of Fig. 5 under various experimental conditions. A comparison between experimental and simulated PIPICO curves indicates that CH_4^{2+} in the $^3T_1$ state dissociates into $CH_3^+ + H^+$ (see Fig. 3). As noted in Sec. III B, we observed very little change in the PIPICO curves over the 35.3–38.5-eV excitation-energy range, i.e., below the second CH_4^{2+} electronic state. Only a slight increase with energy of the risetime of the PIPICO curve at Δt_{min} and Δt_{max} values of Δt was noted. The nonzero risetime is due to the distribution of the total kinetic energy E_{kin} of the fragments. Therefore the mean value and the width of this distribution can be estimated by comparing the experimental PIPICO curve with calculated curves simulated with various kinetic energies (see Fig. 4). We thus obtained $E_{kin} = 5.3 \pm 1.1$ eV, at 37-eV excitation energy. The relatively wide distribution of the kinetic energy may be due to the combination of two effects: (i) the broad Franck-Condon energy region for excitation of the $CH_4^{2+}(^3T_1)$ state as discussed in Sec. III B; (ii) distribution of the internal (vibration and rotation) energy of the CH_3^+ product.

From these results we conclude that the energy for formation of the products $CH_3^+ + H^+$ issuing from the dissociation of the $^3T_1$ state is 31.7±1.1 eV. It follows (see Table IV) that the CH_3^+ fragment is most probably produced in its electronic ground state $\tilde{X}\,^1A_1$, with a mean internal energy of about 3.9±1.1 eV. These $CH_3^+(\tilde{X}\,^1A_1') + H^+$ (Ref. 3) products are correlated to the $^1A_1$ state of CH_4^{2+} whose vertical energy is calculated to be 42.6 eV (see Table III) so that the dissociation of $CH_4^{2+}(^3T_1)$ into these products is not a direct process, but result from predissociation.

In studying the stability of doubly charged CH_4^{2+} cations, Siegbahn[21] remarked that, both energetically and dynamically, the $CH_3^+ + H^+$ dissociation channel should be the most favorable pathway for dissociation, as compared to other channels such as $CH_2^+ + H_2^+$, $CH^+ + H_3^+$, etc. This prediction agrees with our observations concerning dissociation of the $^3T_1$ state. We note that the $^3T_1$-state energies reached in the PIPICO experiment are in the neighborhood of the vertical energy at 37.15 eV, i.e., well above the D_{4h} structure barrier at 33.4 eV for dissociation into $CH_3^+ + H^+$ as calculated by Siegbahn[21] (there is no barrier in the T_d structure[22]). A rapid dissociation is thus expected in this case. The exact dissociation pathway may be complex. Siegbahn considered that CH_4^{2+} begins to dissociate along the $CH_3^{2+} + H$ attractive potential-energy curve until the latter intersects with the strongly repulsive $CH_3^+ + H^+$ curve where an electron jump results in the ion dissociating into CH_3^+ and H^+.

2. Dissociation of CH_4^{2+} in its ^1E state

For excitation energies above 38.5 eV, the PIPICO curves differ from that corresponding to the $^3T_1$ state. This is shown in Fig. 10 which gives a PIPICO curve recorded at 42 eV under the same experimental conditions as that in curve *a* of 4 measured at 38.5 eV. At an excitation energy of 42 eV, the PIPICO signal is the sum of the signals corresponding to the $^3T_1$ state and the ^1E state. The weight of each in the sum is determined by the cross section for formation of the corresponding CH_4^{2+} electronic state at 42 eV. In order to subtract the contribution of the $^3T_1$ state from the PIPICO curve of Fig. 10, we determined the cross section for formation of this state at 42 eV by a linear extrapolation of that part of the σ^{2+} curve (see Figs. 7 and 8) which lies between 37.15 and 38.5 eV. After subtraction, the PIPICO curve *a* of Fig. 11 is obtained, which corresponds to the dissociation of the sole ^1E state.

Determination of the ^1E-state dissociation process is done by comparison of the experimental PIPICO curve with simulated ones. As compared to the PIPICO curve of Figs. 3, curve *a* and 4, curve *a* which corresponds to the $CH_3^+ + H^+$ process, curve *a* of Fig. 11 is shifted towards lower channels. We recall here that the $(\Delta t_{max} + \Delta t_{min})/2$ value was observed (Sec. II A) to depend only on the dissociation process and not on the kinetic energy released. After simulating the PIPICO curves of various dissociation processes (see Table IV), we concluded that the ^1E-state PIPICO curve was best fitted by the simulated curve corresponding to the $CH_4^{2+} \rightarrow CH_2^+ + H^+ + H$ channel. This dissociation process is the only one which

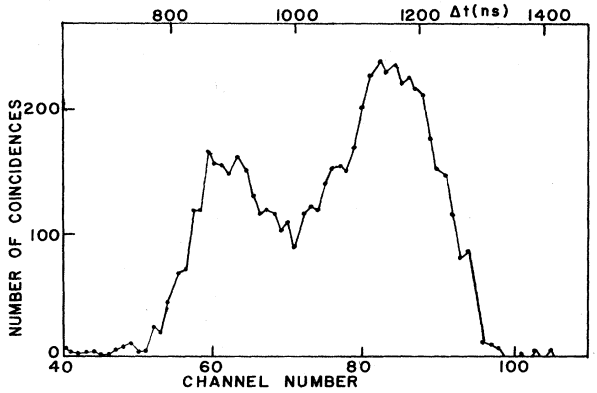

FIG. 10. Experimental PIPICO curve at a 42-eV photon excitation energy. Extraction electric field is 30 V/cm. Ion count rate is 1000/s. Time of accumulation is 1.2 h.

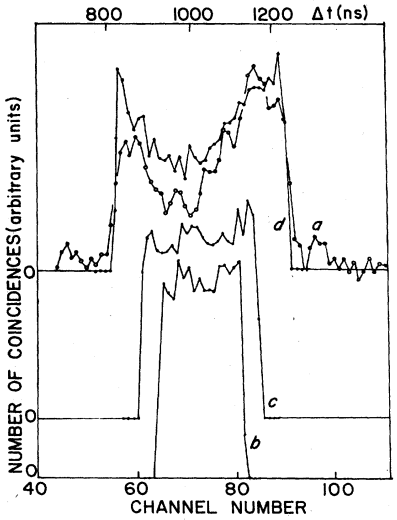

FIG. 11. Curve *a*: Experimental PIPICO curve at a 42-eV photon excitation energy, obtained as explained in the text, and corresponding to dissociation of the ^1E state of CH_4^{2+}. Curve *b*: Simulated PIPICO curve corresponding to the $CH_4^{2+} \rightarrow CH_2^+ + H^+ + H$ dissociation channel, within the statistical model. Curve *c*: Same as *b* but within the impulsive model. Curve *d*: Same as *b* but within the Coulomb repulsion model.

gives a $(\Delta t_{max} + \Delta t_{min})/2$ value which agrees with the experimental one, as can be seen in curves *b*, *c*, and *d* of Fig. 11. Other dissociation processes, some of which are represented in curves *c* and *e* of Fig. 3, were found not to agree with experimental results.

The dissociation of CH_4^{2+} into three products $CH_2^+ + H^+ + H$ is more complicated than dissociation into two products as studied in Sec. III C 1. Conservation of momentum and energy is no longer sufficient to determine the partition of the total momentum and kinetic energy into the products. We therefore investigated some additional hypotheses. Three different models were considered.

(i) *Statistical model.* Baer *et al.*[48] recently studied statistical energy partitioning in the dissociation process leading to several products. Their model is directly applicable to the $CH_4^{2+} \rightarrow CH_2^+ + H^+ + H$ dissociation, if we assume that the internal energy of CH_4^{2+} is statistically distributed over all the degrees of freedom of the fragments. Considering that rigorous energy conservation can be replaced by average energy conservation, Baer *et al.* derived simple relations for calculating the average kinetic energy of each fragment, the average internal energy of molecular fragments, and the average angles between the velocity vectors of the fragments. By assuming that the dissociation of CH_4^{2+} is simultaneous and that the average values can be taken as unique values of the kinetic energy E_{kin} of the fragments and of the angles θ' between their velocity vectors, one obtains the following parameters:

$$E_{kin}(H^+) = 0.18E^* ,$$
$$E_{kin}(CH_2^+) = 0.024E^* ,$$
$$\theta'(H^+, CH_2^+) = 133.1^\circ .$$

E^* is the $CH_4^{2+}(^1E)$-state energy above the dissociation limit $CH_2^+ + H^+ + H$ at 33.3 eV (see Table IV) and is equal to 5.2 eV.

Using the procedure described in Sec. II A, we obtained the PIPICO curve *b* of Fig. 11. It is clear that both the Δt_{max} and Δt_{min} values and the relative height of the middle part of this curve disagree with the experimental curve *a* of Fig. 11.

(ii) *Impulsive model.* In this very simplified classical model we made the following assumptions: the momenta of fragments H^+ and H have the same intensity and are directed along the C—H bonds. Within these approximations we obtain

$$E_{kin}(H^+) = 0.48E_t ,$$
$$E_{kin}(CH_2^+) = 0.045E_t ,$$
$$\theta'(H^+, CH_2^+) = 125.3^\circ .$$

The total kinetic energy released E_t was taken equal to 5 eV in order to best fit the experimental PIPICO curve *a* of Fig. 11. However, we see that the simulated curve, curve *c* of Fig. 11, does not fit the experimental curve at all. Smaller values of E_t would increase this disagreement by decreasing the width of the PIPICO curve.

(iii) *Coulomb repulsion model.* It is clear from the preceding results that in order to obtain a good fit of the experimental PIPICO curve, we have to increase, in our simulation, the angle $\theta'(H^+, CH_2^+)$ between the initial velocity vectors of H^+ and CH_2^+. This would increase the width of the simulated curve and also depress the curve in the middle. A reasonably good fit occurs with curve *d* of Fig. 11. It was obtained by assuming that $\theta'(H^+, CH_2^+) = 180^\circ$ and that almost all the available energy E^* is released as kinetic energy of ionic fragments H^+ and CH_2^+, the neutral H fragment having no kinetic energy. The parameters used to obtain the simulated curve *d* of Fig. 11 are as follows:

$$E_{kin}(H^+) = 0.93E_t ,$$
$$E_{kin}(CH_2^+) = 0.07E_t ,$$
$$\theta'(H^+, CH_2^+) = 180^\circ ,$$
$$E_t = 5 \text{ eV} .$$

We note that in the simulated curves *b*—*d* of Fig. 11, the $(\Delta t_{min} + \Delta t_{max})/2$ value is independent of the dissociation model. This confirms that this value only depends on the dissociation channel. Although the fit of the experimental PIPICO curve is not as good as in the case of the $^3T_1$ state (see curves *a* and *b* of Fig. 3), the fit obtained within the Coulomb repulsion model is the best that we could obtain. This indicates that dissociation models of the statistical or impulsive type, which are usually used to explain the dissociation of neutral or singly ionized molecules, are inadequate in the case of the dissociation of CH_4^{2+} in its ^1E state. In this case Coulomb repulsion between the two ionic fragments H^+ and CH_2^+ seems to play the dominant role in the fragmentation process.

IV. CONCLUSION

As indicated in the Introduction, the energies of electronic states of the doubly charged CH_4^{2+} cation are not sensitive to electron correlations. More appropriate probes of the electron correlations are knowledge of (i) which CH_4^{2+} states are populated, (ii) the probability (cross section) of their formation, and finally, (iii) the shape of the σ^{2+} curve as a function of the photon excitation energy. We emphasize, however, that comparison with theory is necessary in order to understand in detail the role of electron correlation in DPI. There is, at the present time, a strong need for extending molecular single-ionization theoretical studies to the case of double photoionization.

Concerning the dissociation of doubly charged cations, we remark that, using the PIPICO method, we are able to achieve a state-to-state study of the fragmentation processes. Furthermore, this method is well suited for obtaining detailed information on fragmentation into more than two products. These seem to be common processes in doubly charged molecular cations. Theoretical studies are also necessary in this field, in particular to determine the role of Coulomb repulsion between positive charges in the dissociation into ionic products; this repulsion force appears to be important, as shown in the case of CH_4^{2+}.

---

*Laboratoire propre du Centre National de la Recherche Scientifique.

[1]G. Dujardin, S. Leach, O. Dutuit, P. M. Guyon, and M. Richard-Viard, Chem. Phys. **88**, 339 (1984).

[2]W. Eberhardt, T. K. Sham, R. Carr, S. Krummacher, M. Strongin, S. L. Weng, and D. Wesner, Phys. Rev. Lett. **50**, 1038 (1983).

[3]G. Bieri and L. Åsbrink, J. Electron Spectrosc. Relat. Phenom. **20**, 149 (1980).

[4]M. J. Van der Wiel, W. Stoll, A. Hamnett, and C. E. Brion, Chem. Phys. Lett. **37**, 240 (1976).

[5]G. V. Marr and R. M. Holmes, J. Phys. B **13**, 939 (1980).

[6]R. Spohr, T. Bergmark, N. Magnusson, L. O. Werme, C. Nordling, and K. Siegbahn, Phys. Scr. **2**, 31 (1970).

[7]U. Gelius, J. Electron Spectrosc. Relat. Phenom. **5**, 985 (1974).

[8]W. Eberhardt, R. P. Haelbich, M. Iwan, E. E. Koch, and C. Kunz, Chem. Phys. Lett. **40**, 180 (1976).

[9]J. J. Pireaux, S. Svensson, E. Basilier, P. A. Malmqvist, U. Gelius, R. Caudano, and K. Siegbahn, Phys. Rev. A **14**, 2133 (1976).

[10]D. Moncrieff, I. H. Hillier, S. A. Pope, and M. F. Guest, Chem. Phys. **82**, 139 (1983).

[11]R. Locht, J. L. Olivier, and J. Momigny, Chem. Phys. **43**, 425 (1979).

[12]A. F. Saturno, Theor. Chim. Acta **7**, 273 (1967).

[13]K. E. McCulloh, T. E. Sharp, and H. M. Rosenstock, J. Chem. Phys. **42**, 3501 (1965).

[14]C. Backx and M. J. Van der Wiel, J. Phys. B **8**, 3020 (1975).

[15]J. Appell, J. Durup, F. C. Fehsenfeld, and P. Fournier, J. Phys. B **7**, 406 (1974).

[16]E. Clementi and H. Popkie, J. Am. Chem. Soc. **94**, 4057 (1972).

[17]I. B. Ortenburger and P. S. Bagus, Phys. Rev. A **11**, 1501 (1975).

[18]T. Ast, C. J. Porter, C. J. Proctor, and J. H. Beynon, Chem. Phys. Lett. **78**, 439 (1981).

[19]M. Rabrenovic, A. G. Brenton, J. H. Beynon, Int. J. Mass Spectrom. Ion Phys. **52**, 175 (1983).

[20]A. W. Hanner and T. F. Moran, Org. Mass Spectrom. **16**, 512 (1981).

[21]E. M. Siegbahn, Chem. Phys. **66**, 443 (1982).

[22]J. A. Pople, B. Tidor, and P. R. Schleyer, Chem. Phys. Lett. **88**, 533 (1982).

[23]R. Stockbauer, J. Chem. Phys. **58**, 3800 (1973).

[24]J. Berkowitz, *Photoabsorption, Photoionization and Photoelectron Spectroscopy* (Academic, New York, 1979), p. 271.

[25]P. L. Kronebusch and J. Berkowitz, Int. J. Mass Spectrom. Ion Phys. **22**, 283 (1976).

[26]J. Appell, thèse du Docteur-ès-Sciences, Université de Paris—Sud (Orsay), 1972.

[27]L. C. Lee, R. W. Carlson, D. L. Judge, and M. Ogawa, J. Quant. Spectrosc. Radiat. Transfer **13**, 1023 (1973).

[28]R. S. Berry and S. Leach, Adv. Electron. Electron Phys. **57**, 1 (1981).

[29]T. Masuoka and J. R. Samson, J. Chim. Phys. **77**, 623 (1980).

[30]V. Schmidt, N. Sandner, H. Kuntzemüller, P. Dhez, F. Wuilleumier, and E. Källne, Phys. Rev. **13**, 1748 (1976).

[31]D. M. P. Holland, K. Codling, J. B. West, and G. V. Marr, J. Phys. B **12**, 2465 (1979).

[32]T. A. Carlson, Phys. Rev. **156**, 142 (1967).

[33]M. J. Van der Wiel and G. Wieber, Physica (Utrecht) **54**, 411 (1971).

[34]G. R. Wight and M. J. Van der Wiel, J. Phys. B **9**, 1319 (1976).

[35]G. Dujardin, D. Winkoun, and S. Leach (unpublished).

[36]G. H. Wannier, Phys. Rev. **90**, 817 (1953).

[37]F. H. Dorman and J. D. Morrison, J. Chem. Phys. **34**, 1407 (1961).

[38]F. H. Dorman and J. D. Morrison, J. Chem. Phys. **35**, 575 (1961).

[39]G. Herzberg, *Electronic Spectra and Electronic Structure of Polyatomic Molecules* (Van Nostrand, New York, 1966).

[40]J. D. Morrison and A. J. C. Nicholson, J. Chem. Phys. **31**, 1320 (1959).

[41]H. P. Kelly, Phys. Rev. **131**, 684 (1963).

[42]J. Dyke, N. Jonathan, E. Lee, and A. Morris, J. Chem. Soc. Faraday Trans. 2 **72**, 1397 (1976).

[43]W. A. Chupka, J. Chem. Phys. **48**, 2337 (1968).

[44]V. H. Dibeler, M. Krauss, R. M. Reese, and F. N. Harlee, J. Chem. Phys. **42**, 3791 (1965).

[45]K. P. Huber and G. Herzberg, *Constants of Diatomic Molecules* (Van Nostrand Reinhold, New York, 1979).

[46]C. E. Moore, *Atomic Energy Levels,* Natl. Bur. Stand. (U.S.) Circ. No. 467 (U.S. GPO, Washington, D.C., 1949).

[47]G. Dujardin, T. Govers, S. Leach, and D. Winkoun, 38th International Meeting of the Societé de Chimie Physique, Bombannes, 17—21 September, 1984 (unpublished).

[48]T. Baer, A. E. DePristo, and J. J. Hermans, J. Chem. Phys. **76**, 5917 (1982).